VNU Journal of Science: Mathematics – Physics, Vol. 42, No. 1 (2026) 67-77

VNU Journal of Science: Mathematics - Physics

Journal homepage: https://js.vnu.edu.vn/MaP

Original Article

Numerical Study on Micro-optical Vortex Generation with the Use of an Achromatic Nanostructured Phase Mask

Nguyen Thuy Linh[1], Nguyen Thanh Tung[1], Le An Khanh[2], To Gia Khanh[2], Tran Thi Hai[1], Chu Van Bien[3], Nguyen Thi Hue[1,*]

[1]*Hong Duc University, 565 Quang Trung, Thanh Hoa, Vietnam*

[2]*Lam Son High School for the Gifted, 307 Le Lai, Thanh Hoa, Vietnam*

[3]*Yersin Da Lat University, 27 Ton That Tung, Lam Vien, Da Lat, Vietnam*

Received 4th September 2025
Revised 29th October 2025; Accepted 02nd March 2026

Abstract: We present the design and numerical evaluation of an achromatic, nanostructured vortex phase micro-optical mask and a numerical analysis of its optical function to generate fundamental charged optical vortex beams in the visible and near-infrared spectral regions. The nanostructured mask was designed using a pair of thermally compatible commercial glasses, enabling cost-effective production through an adapted stack-and-draw technique. An initial investigation was conducted on 20 µm-thick free-space achromatic vortex phase mask designs. The results confirmed successful vortex beam generation with a fundamental topological charge, with mode-conversion efficiencies reaching 100% at wavelengths of 542 nm and 773 nm. Furthermore, the mask demonstrated the ability to correct chromatic aberration, achieving over 90% mode-conversion efficiency across a broad spectrum (bandwidth of 416 nm) from 504 nm to 920 nm. These results highlight the potential of this achromatic nanostructured vortex mask for integrated broadband vortex beam generation in applications such as optical trapping, high-resolution microscopy, and laser micromachining.

Keywords: Micro-optical vortex, nano-structurization, achromatic mask.

1. Introduction

Optical vortex (OV) beams are characterized by a toroidal intensity distribution and a helical wavefront with a phase singularity, imparting orbital angular momentum (OAM) of $l\hbar$ per photon [1, 2]. Their phase structure is described by the vortex phase factor $\exp(il\theta)$, where l is the topological

* Corresponding author.
E-mail address: nguyenthihuevl@hdu.edu.vn

https//doi.org/10.25073/2588-1124/vnumap.5074

charge that dictates the OAM magnitude, and θ represents the angular angle. Due to these distinctive features, vortex beams have enabled breakthroughs in optical trapping and micromanipulation [3, 4], super-resolution microscopy (e.g., STED) [5, 6], high-capacity optical communications (via OAM multiplexing) [7, 8], laser material processing [9], and quantum state encoding [10].

Since some of these applications use broadband light sources, maintaining a consistent spatial beam profile and angular momentum across all spectral masks can be challenging. To address this, vortex generation must employ an achromatic device or setup. Additionally, when the light source is a laser emitting ultrashort and ultraintense pulses, the components used must withstand high damage thresholds while preserving the pulse's duration and shape without causing distortion. While established methods, such as spiral phase plates [11, 12], spatial light modulators [13, 14], and Q-plates [15]. These traditional components are widely used to generate vortex beams, but their complex geometries typically lead to bulky setups, high production costs, and limited performance scalability.

In this study, we propose and thoroughly simulate an achromatic nanostructured gradient-index (GRIN) vortex phase mask (AnVPM) designed for the efficient generation of broadband optical beams carrying a fundamental topological charge. Our approach relies on material nanostructuring combined with effective medium theory [16, 17], enabling the realisation of arbitrary transverse refractive index profiles by tuning glass dispersion and precisely arranging glass nanorods [18-20]. The concept that a flat, binary nanostructure with a transverse index profile varying linearly with the azimuthal angle can produce monochromatic OAM beams has been previously validated both theoretically and experimentally [18, 21]. This methodology was also successfully used in creating a broadband nanostructured GRIN vortex phase element, reaching over 90% mode-conversion efficiency across a 416 nm bandwidth in the near-infrared spectrum. We expand the concept by proposing and numerically analysing achromatic nanostructured GRIN vortex masks for generating OV beams with a single topological charge, achieving a mode-conversion efficiency of up to 100% at two representative laser wavelengths. As a proof of concept, we conducted numerical simulations to assess the performance of a selected free-space AnVPM sample with a thickness of 20 μm, demonstrating effective chromatic aberration correction at two different wavelengths. Moreover, we examined its broadband performance with a high mode-conversion efficiency exceeding 90% spanning the visible to near-infrared range.

2. Development of Achromatic Nanostructured Phase Mask

The main principle of a nanostructured gradient-index vortex phase mask (nVPM) involves designing the distribution of nanorods made of two thermally matched glasses in such a way that the cross-sectional effective refractive index profile of the nVPM, based on effective medium theory, varies linearly with the azimuthal angle while remaining uniform along the radial direction. Such a refractive index gradient induces a spiral phase modulation on the incoming fundamental beam. As a result, the nVPM produces a vortex beam characterised by a topological charge l and an associated helical phase shift:

$$\Delta\varphi = 2\pi l = 2\pi \frac{\Delta n(\lambda)}{\lambda} d \, . \tag{1}$$

where Δn represents the difference in refractive index between its maximum and minimum values (two glass indices), which varies with the operating wavelength λ. For a vortex beam with a single topological charge (l = 1), a total phase shift of 2π is required. This leads to a simplified expression of Eq. (1): $d = \lambda/\Delta n(\lambda)$, which can be used to determine the mask's thickness at a specific wavelength. In earlier studies [21], the nanostructured vortex phase masks demonstrated only monochromatic functionality – each nVPM was designed with a precise thickness tailored to operate at a particular wavelength λ¬0. This is

easily noticeable in Fig. 1(a), which illustrates the mono-dependence of phase shift on wavelength for generating optical vortex beams with a fundamental topological charge using NC-borosilicate glasses.

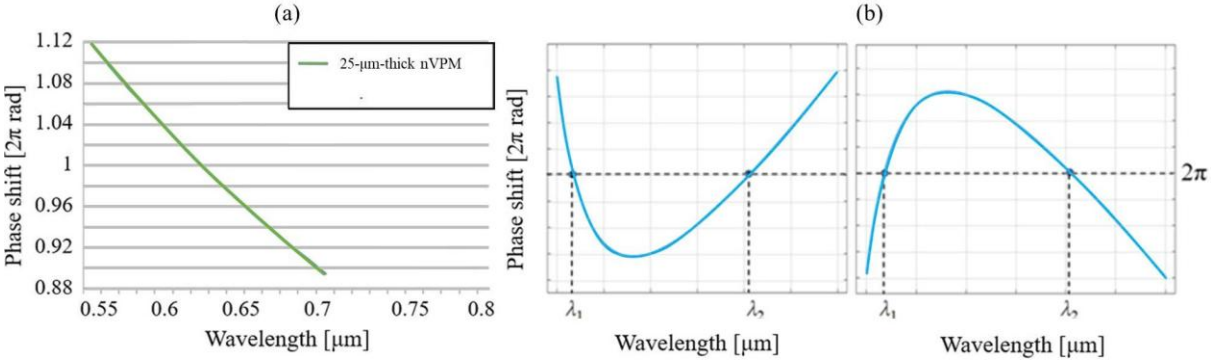

Figure 1. Illustration of the monochromatic characteristic of the NC-glass nVPM [21] (a) and the achromatic attribute of the target AnVPM (b) for the generation of charge-1 OV beams.

This study aims to design a novel nanostructured vortex phase mask with achromatic properties capable of producing vortex beams with charge one at specific pairs of wavelengths. In this context, achromaticity means that an AnVPM with a fixed thickness d_0 can generate optical vortex beams with the same topological charge across multiple wavelengths. Specifically, this requires the phase shifts at two different wavelengths, λ_1 and λ_2, to be identical. This condition underscores the necessity of compensating chromatic aberration at these wavelengths to create single-charge optical vortex beams effectively. For example, the phase shift as a function of wavelength should follow a second-order polynomial form, as shown in Fig. 1(b), indicating that identical values occur at specific pairs of wavelengths. Based on Eq. (1), the corresponding refractive index condition is derived as follows:

$$\boldsymbol{\Delta\varphi_1 = \Delta\varphi_2 \rightarrow 2\pi d_0 \frac{\Delta n(\lambda_1)}{\lambda_1} = 2\pi d_0 \frac{\Delta n(\lambda_2)}{\lambda_2} \rightarrow \frac{\Delta n(\lambda_1)}{\lambda_1} = \frac{\Delta n(\lambda_2)}{\lambda_2}}. \quad (2)$$

This implies that the ratio $\frac{\Delta n(\lambda)}{\lambda}$ must remain constant at a minimum of two different wavelengths (e.g. the $(\Delta n(\lambda))/\lambda$ curves exhibit parabolic profiles). To satisfy this condition, it is necessary to tailor the dispersion curves of the glass materials used for the realization of the binary nanostructured mask. Consequently, selecting a pair of glasses with well-matched dispersion characteristics, along with careful design of a binary nanostructure composed of nano-rods from these materials, is essential. Moreover, to be compatible with the stack-and-draw fabrication method, the selected glass pair must also exhibit suitable rheological behaviour and have closely matched thermal expansion coefficients to ensure compatibility during fiber drawing and to prevent the formation of internal stress after the process. This is discussed in more detail in the report of the concept of AnVPM in [22].

In this work, we propose using existing soft glasses labelled H-ZlaF89L and H-ZF62 as the high-refractive-index and low-refractive-index materials, respectively. These glasses were produced by the company CDGM [23]. H-ZlaF89L and H-ZF62 offer high optical transmission across (> 90 % for all considered wavelengths) a wide wavelength range, from the visible spectrum to the mid-infrared (420 nm – 2400 nm), as shown in Fig. 2. Importantly, the glasses have comparable thermal and physical properties, as detailed in Table 1. This allows the possibility of fabrication of the developed micro-optical masks using the nanostructuring technique realized by the stack-and-draw method [18, 24]. As a previous demonstration of the development of nGRIN microlenses with achromatic correction in the near-infrared region using two types of custom-tailored borosilicate glasses [25] and Lead–Bismuth–

Gallium silicate ultra-thin nanostructured vortex elements [26] for broadband micro-optical vortex generation. Indeed, H-ZlaF89L and H-ZF62 glasses exhibit comparable thermal and rheological behaviours. Table 1 shows that the difference in thermal expansion coefficients (Δα) between H-ZlaF89L and H-ZF62 reaches 11×10^{-7} K^{-1}. The transformation temperature ($\mathbf{T_g}$) and Sag temperature ($\mathbf{T_s}$) are closely matched, with the difference being 12 °C and 6 °C, respectively. Viscosity-related temperatures, including strain point, annealing point, and softening point of those glasses, are very similar. These small differences, all within the acceptable 20 °C processing window, suggest that both glasses can be co-processed under similar thermal conditions for multi-material optical fiber fabrication.

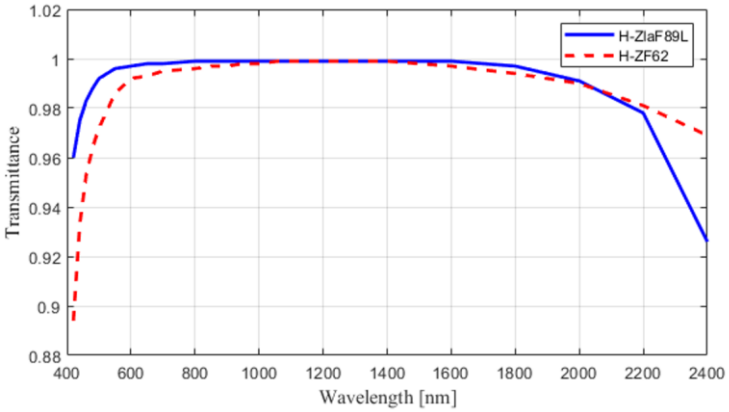

Figure 2. Transmission characteristics of H-ZlaF89L glass and H-ZF62 glass (the sample thickness of 5 mm) in the considered wavelength range.

Table 1. Physical and thermal parameters of H-ZlaF89L and H-ZF62 glasses

Parameters	H-ZlaF89L	H-ZF62
Thermal Expansion Coefficient $\alpha_{100/300^oC}$ [10^{-7} K^{-1}]	88	77
$\alpha_{-30/70^oC}$ [10^{-7} K^{-1}]	72	64
Transformation temperature T_g [°C]	708	720
Sag Temperature $\mathbf{T_s}$ [°C]	745	751
Strain Point $\mathbf{T_{10}^{14.5}}$ [°C]	649	667
Annealing Point $\mathbf{T_{10}^{13}}$ [°C]	685	699
Softening Point $\mathbf{T_{10}^{7.6}}$ [°C]	800	806

The dispersion characteristics of H-ZlaF89L and H-ZF62 glasses are numerically performed in Fig. 3 (a, b). The data reveal a nonlinear increase in index contrast with wavelength (Fig. 3(b)) – rapid in the visible spectrum and more gradual in the near-infrared – resulting in a Δn/λ curve with a parabolic trend, represented in Fig. 3(c). This behaviour enables the achromatic performance of the designed AnVPM.

The achromatic property of the nanostructured gradient index vortex phase mask (AnVPM) is determined by its nanorod spatial configuration and the refractive index profiles of the selected glass pair. The designed binary structure of the AnVPM consists of 13267 nano-rods arranged in a hexagonal lattice, with 133 rods along its longest diagonal, as represented in Fig. 4(a). The resulting designed mask has an overall diameter of approximately 20 μm, which corresponds to an individual nano-region size of about D = 150 nm. Based on the boundary conditions from effective medium theory, the incident

light perceives the nanostructured element as a uniform medium when the wavelength exceeds $\lambda_0 = D \times 2\pi$. However, this theoretical limit does not account for material diffusion during thermal processes, which smooths the boundaries between nanorods. As a result, the practical lower wavelength limit for the effective medium approximation shifts to $\lambda_0 = D \times 3 = 450$ nm. In this work, for all wavelengths $\lambda \geq 450$ nm, the nanostructured achromatic vortex mask can produce an effective refractive index distribution that closely mimics that of the target one, e.g. the ideal continuous-index vortex phase mask (AVPM), as in Fig. 4(b).

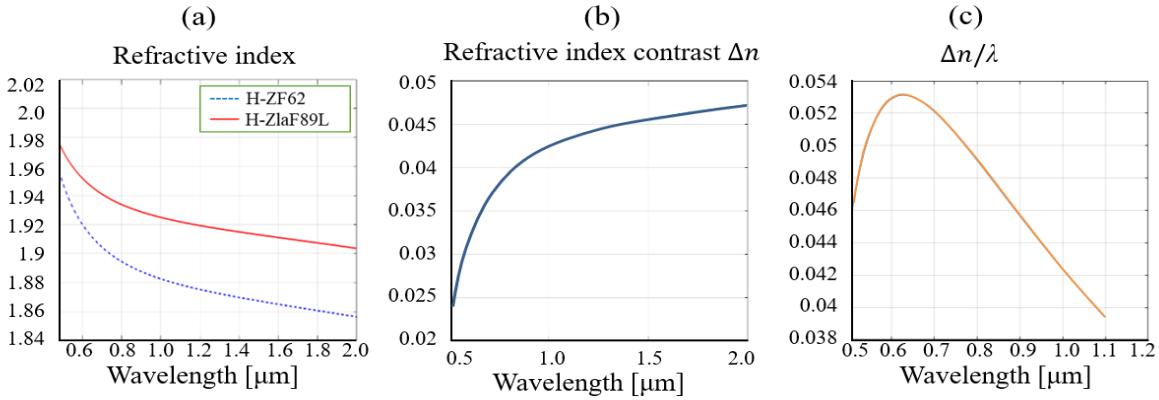

Figure 3. H-ZlaF89L glass and H-ZF62 glass refractive indices (a) and their index contrast as a function of wavelengths (b) in the visible and near-infrared regions.

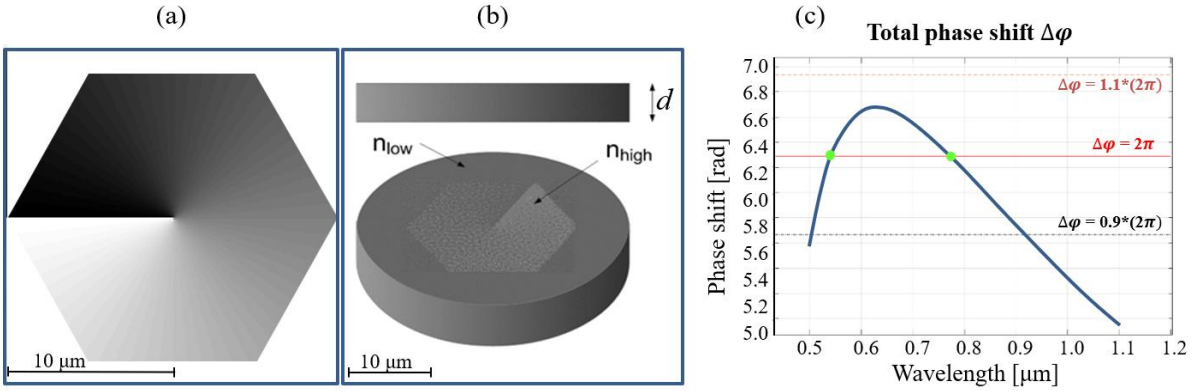

Figure 4. (a) The ideal continuous refractive index distribution of the achromatic phase mask, (b) the designed AnVPM with the central corresponding vortex nanostructure, and (c) the total phase shift modulated by the component with a thickness of 20 μm following wavelengths.

As an initial test, this work theoretically and numerically examines a cylindrical component with a thickness of 20 μm for the generation of OV beams in visible and near-infrared regions. The AnVPM features a central vortex nanostructure in a regular hexagonal lattice with a long diagonal of 20 μm. It is surrounded by a cladding made of lower-index glass to form the component of a total diameter of 125 μm, ensuring compatibility with the fiber integration for potential applications in all-fiber system.

Based on Eq. (1), we calculated the total phase shift created by the AnVPM, as illustrated in Fig. 4(c). It can be seen that the proposed vortex mask can create a slightly changed total phase shift

following wavelengths, which increases quickly from green light to red light, then reduces gradually for longer wavelengths. It reaches the maximum of $\Delta\varphi = 1.06(2\pi)$ at the wavelength of 628 nm. In detail, we obtained a total phase shift of exactly 2π (topological charge $l = 1$, e.g. efficiency of over 100 %) at two wavelengths, $\lambda_1 = 542$ nm and $\lambda_2 = 773$ nm, shown by two green dots in Fig. 4(c). Moreover, OV beams with the same single topological charge can still be achieved, with an error margin of $\Delta l = 0.1$ (e.g., efficiency of over 90 %). This is based on careful theoretical analysis combined with experimental work on broadband nVPMs [26]. Fig. 4(c) shows that the AnVPC is theoretically capable of generating fundamental charge vortices with the efficiency of over 90 % within a wavelength range from 504 nm to 920 nm, a bandwidth of 416 nm spanning from visible to near-infrared regimes.

3. Numerical Characterization of the Designed Mask

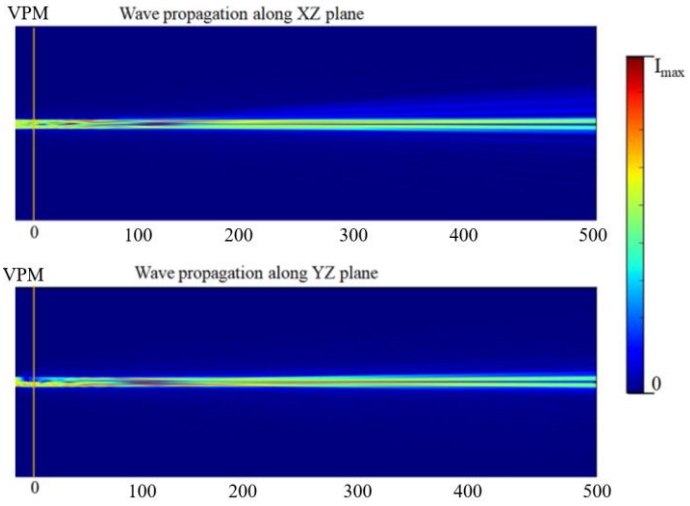

Figure 5. Example of modelling light propagation in the designed vortex structure and then over a 500-μm distance in free space along the *z-axis*.

To simulate the performance of the designed achromatic nanostructured gradient index vortex phase mask, we employed the Fourier Transform-based Beam Propagation Method [27]. In principle, the incident beam propagates through the considered vortex structure and then in free space. In our simulations, the simulated parameters of the designed structure are described in the previous section. Simulations modelled the propagation of light through the nanostructured mask, followed by 1000 μm of air, as an example of light propagation modelling shown in Fig. 5. The computational domain measured 600 × 600 × 1100 μm in the x, y, and z directions, respectively. To maintain accuracy, a uniform spatial step size of 0.1 μm was used along both the x- and y-axes throughout the entire domain. Along the optical (z-) axis, step sizes varied by region: 0.1 μm within the AnVPM structure and 0.5 μm in the air. All output fields were analysed at a propagation distance of 1000 μm beyond the mask's exit surface. The simulated OVBS' field intensity and phase distributions will be visualized at the end of the simulation area.

The first simulation set is designed to determine the optimal incident beam size for interacting with vortex mask designs, thereby achieving a uniform intensity distribution of OV beams. To do this, we numerically tested various pinhole sizes, e.g. 12, 15, 18, 20, 23, and 30 μm. In this simulated set, it is sufficient to simulate only for the ideal continuous masks, which feature a structural diameter of 20 μm.

The modelled OV beams obtained at a wavelength of 542 nm are presented in Fig. 6. The simulated results show that, in all cases, the created beam exhibits doughnut-like intensity distributions and correct single twist phase structures (except for the case of the big incident beams, as shown in Fig. 6(f,g)). However, it is visible that the OV beams with the most uniform characteristics result from converting an Gaussian beam with the size similar to the AVPM's aperture (20 μm) . That means the incident beam should be assumed to have a diameter of from 18 to 20 μm to ensure efficient interaction with the vortex-generating structure. A beam that is too narrow fails to sample the azimuthal index variation near the centre of the AnVPM, making OVB formation ineffective. Conversely, a beam significantly wider than the aperture results in most light passing the mask, degrading the quality of the transmitted vortex beam. The findings confirm that optimal OVB generation occurs when the beam diameter is slightly smaller than the mask's aperture.

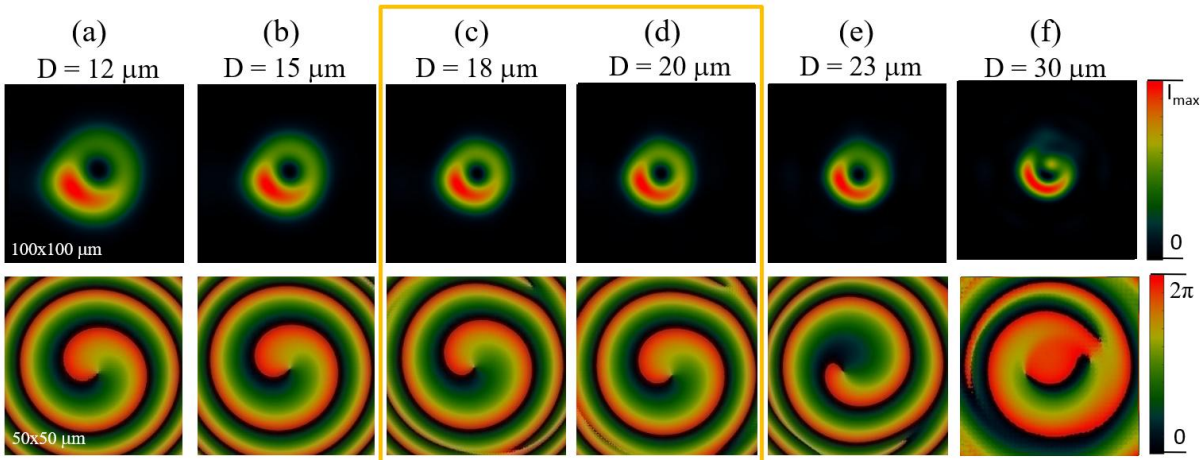

Figure 6. Numerical calculation of the field and phase of OV beams for several incident-beam size cases using the designed continuous index AVPM.

In the next series of simulations, we examined the optical performance of the proposed designs, which were theoretically predicted to convert Gaussian beams into single-charge OV beams with mode-conversion efficiencies reaching 100% at two calculated wavelengths λ_1 = 542 nm and λ_2 = 773 nm. At λ_1 = 542 nm, the refractive indices of H-ZlaF89L and H-ZF62 are 2.0110 and 1.9344, respectively. At λ_2 = 773 nm, the corresponding indices are 1.9770 for H-ZlaF89L and 1.8968 for H-ZF62. Both the ideal continuous-index AVPM and the nanostructured AnVPM designs were considered for comparison. The results, including the simulated field intensity and phase distributions of the beam after passing through the designed achromatic gradient-index vortex mask, are represented in Fig. 7. It is observable that for the ideal element, see Fig. 7(a), the doughnut-shaped intensity profiles (the first column) display distinct central dark regions, indicating phase singularities and confirming the generation of optical vortices at 542 nm and 773 nm. The corresponding phase maps (the second column) reveal well-defined spiral structures with a single arm, verifying that the topological charge of the vortex beam is l = 1. That means we obtained OV beams with topological charge 1. Spontaneously, Fig. 7(b) shows the output fields generated by the AnVPM, which closely resemble those from the ideal design. This strong agreement demonstrates the ability of the proposed AVPM and AnVPM to produce single-charge vortex beams at both selected wavelengths for an efficiency of 100 %.

Furthermore, the numerical simulations demonstrate that the results for the ideal continuous-index GRIN AVPM and their corresponding binary nanostructured designs are highly consistent. This confirms the accuracy of the nanostructured implementation and its effectiveness in replicating the

performance of an ideal achromatic vortex mask. In other words, the optical performance remains unaffected when employing the nanostructured implementation. Therefore, the AnVPM design has been optimised and is prepared for potential fabrication. It can also be seen that there are still bright spots existing in the intensity profiles of the generated vortex beams, but this is not significantly leading to not-perfect uniform intensity distribution in the beam cross-section. This persists due to waveguiding effects when the light propagates through a certain distance (masks' thickness of 20 μm). It is possible to eliminate this when we reduce the thickness of the AnVPM; however, it is still challenging with the current fabrication technique for thin nVPMs

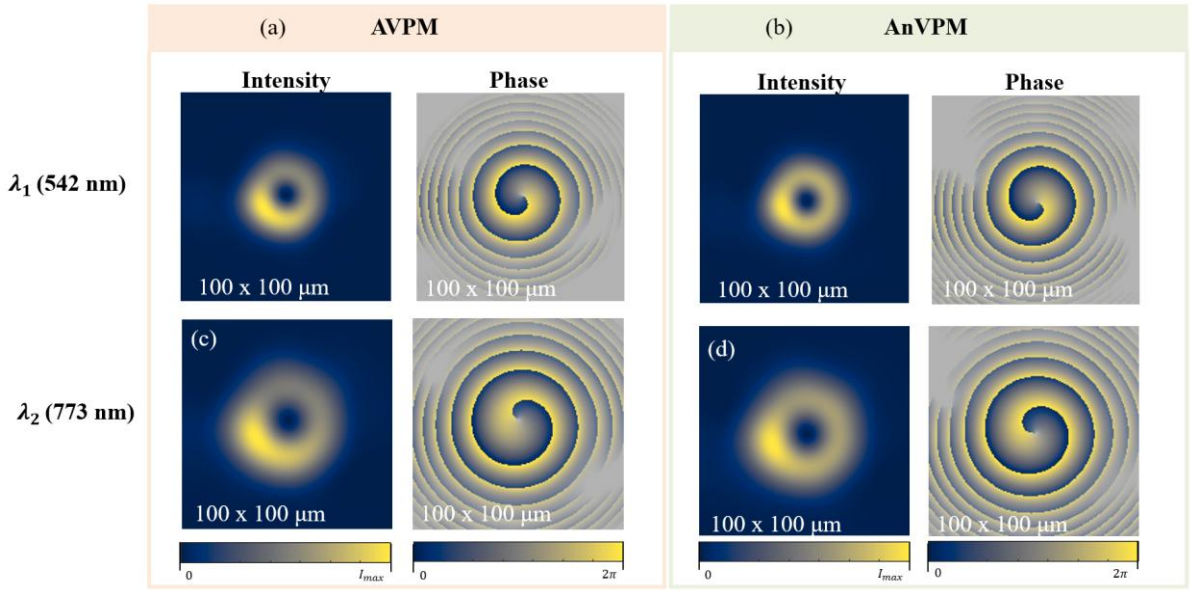

Figure 7. Numerically simulated intensity and phase distributions of the beam generated by the designed A-VPMs with an ideal continuous refractive index profile (a) and a binary nanostructured design (b), at wavelengths of 542 nm (top row) and 773 nm (bottom row).

The second simulation set was conducted for the generation of OV beams, maintaining a topological charge of $l = 1$, with only a minor deviation of $\Delta l = 0.1$. This consistency is attributed to a thorough theoretical analysis supported by experimental investigations conducted on broadband nanostructured gradient index vortex phase masks [26]. The theoretical calculation in Fig. 4(c) predicted that the AnVPM is capable of converting Gaussian beams into fundamental-charge OV beams with conversion efficiency over 90 % across a broad spectral range of 416 nm, specifically from 504 nm to 920 nm.

As previously discussed, the binary nanostructured design shows no performance degradation compared to its ideal continuous-index counterpart. Therefore, in this part, simulations were conducted only for the binary AnVPM structures. These simulations were performed at several selected wavelengths – 504 and 920 nm – where the generated optical vortex beams display topological charges near the boundary values ($l = 1 \pm 0.1$). Additional wavelengths of 628, 732, and 890 nm were included based on the availability of laser sources in our laboratory. All geometric parameters of the AnVPM and simulation and simulation conditions were kept consistent with the earlier calculations. The results of the simulations are shown in Fig. 8. Fig. 8 shows that the intensity distributions in all cases clearly display ring-shaped patterns with a central zero-intensity point. Spontaneously, mono-twists with central phase singularities can be observed in the phase structures of generated OV beams. This evidence demonstrates that we obtained OV beams with a single charge in all cases examined. However, the

uniformity of these intensity patterns is slightly different for the considered wavelengths, with the strongest light localization at the bottom boundary where $l = 0.9$ ($\Delta l = -0.1$), i.e., wavelengths of 504 nm and 920 nm. Indeed, at these boundary wavelengths, the total phase shifts are just under 2π, causing the annular patterns to break, although their phase structure remains intact. This, together with the waveguiding effect, results in a lower quality of the generated OV beams compared to those with a total phase shift of exactly 2π (as described above for two wavelengths $\lambda_1 = 542$ nm and $\lambda_2 = 773$ nm in Fig. 7). Interestingly, at wavelengths corresponding to topological charge values slightly above the standard value $l = 1$ ($\Delta l = 0$ to $+0.1$), the OV beam exhibits a perfect phase distribution and notably improved intensity uniformity. Specifically, at the wavelength of 628 nm ($\Delta l = +0.06$, as shown by the peak of the phase shift curve in Fig. 4(c)), we achieved an almost perfectly uniform intensity distribution across the output beam cross section. The likely scenario is that the winding phase of the generated OV slightly exceeds 2π within this range, resulting in improved beam quality.

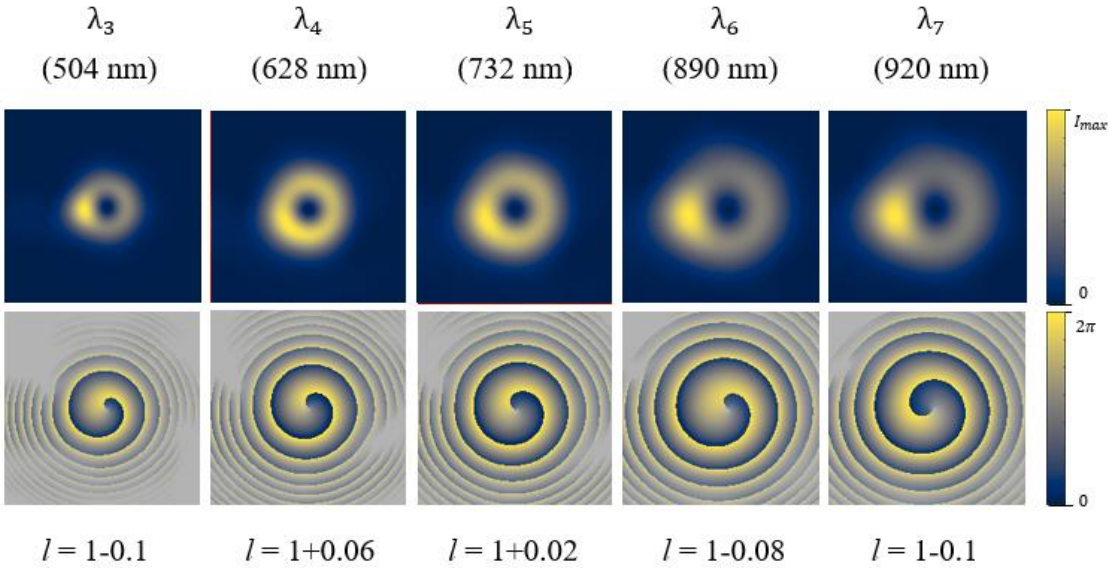

Figure 8. Modelled beam intensity distributions (top row) and corresponding phase structures (bottom row) generated by 20-μm-thick AnVPMs at various wavelengths ranging from 504 nm to 920 nm.

These numerical results agree with theoretical predictions, confirming that the designed achromatic nVPC effectively converts Gaussian beams into fundamental-charge OV beams. It maintains mode-conversion efficiencies above 90% ($l = 1 \pm 0.1$) across a broad spectrum from 504 to 920 nm, covering a bandwidth of 416 nm from the visible to near-infrared regimes. This range is slightly smaller than in the reported case, introducing the concept of AnVPM, but the quality of their beams is much better due to the use of shorter components [22].

4. Conclusions

In this paper, we have reported the development of an achromatic nanostructured gradient index vortex phase mask for the generation of OV beams with fundamental topological charge in a wide wavelength range spanning from visible to near-infrared regions. The mask was developed using two commercial glasses produced by CDGM. These glasses have compatible thermal and dispersion

properties that support achromatic behaviour and the possibility of fabrication of the developed micro-optical masks using the nanostructuring technique realized by the stack-and-draw method. The azimuthal gradient index nanostructure was then created using the simulated annealing algorithm and effective medium theory.

The optical performance of the designed 20-μm-thick AnVPM has been numerically verified by modelling the beam propagation through the designed mask and then in free space based on the Fast Fourier Beam Propagation Method. The simulated results confirmed the effective generation of vortex beams with a single topological charge and a mode-conversion efficiency of 100% at two representative wavelengths of 542 nm and 773 nm. Furthermore, the proposed mask effectively corrects chromatic aberrations, maintaining a high mode-conversion efficiency above 90% over a broad spectral range of 416 nm, spanning from 504 nm to 920 nm. Consequently, the proposed AnVPM not only offers a novel approach for manipulating the orbital angular momentum of photons but also presents practical advantages for micro-optical vortex applications, particularly in integrated optical information processing and optical trapping systems such as optical tweezers

Acknowledgments

This research is funded by Vietnam National Foundation for Science and Technology Development (NAFOSTED) under grant number 103.03-2023.19.

References

[1] Y. Shen, X. Wang, Z. Xie, C. Min, X. Fu, Q. Liu, M. Gong, X. Yuan, Optical Vortices 30 Years on: OAM Manipulation from Topological Charge to Multiple Singularities, Light: Science & Applications, Vol. 8, No. 90, 2019, pp. 1-29, https://doi.org/10.1038/s41377-019-0194-2.

[2] L. Allen, M. W. Beijersbergen, R. J. C. Spreeuw, J. P. Woerdman, Orbital Angular Momentum of Light and The Transformation of Laguerre-Gaussian Laser Modes, Physical Review A, Vol. 45, Issue 11, 1992, pp. 8185-8189, https://doi.org/10.1103/PhysRevA.45.8185.

[3] M. Padgett, R. Bowman, Tweezers with A Twist, Nature Photonics, Vol. 5, Issue 6, 2011, pp. 343-348, https://doi.org/10.1038/nphoton.2011.81.

[4] A. Kocyigit, K. Cicek, R. Topkaya, X. Cai, Integrated Vortex Beam Emitter Device for Optical Manipulation, Applied Optics, Vol. 59, Issue 10, 2020, pp. 3179-3182, https://doi.org/10.1364/AO.384838.

[5] M. Yoshida, Y. Kozawa, S. Sato, Subtraction Imaging by The Combination of Higher-Order Vector Beams for Enhanced Spatial Resolution, Optics Letters, Vol. 44, Issue 4, 2019, pp. 883-886, https://doi.org/10.1364/ol.44.000883.

[6] K. I. Willig, S. O. Rizzoli, V. Westphal, R. Jahn, S. W. Hell, STED Microscopy Reveals That Synaptotagmin Remains Clustered After Synaptic Vesicle Exocytosis, Nature, Vol. 440, Issue 7086, 2006, pp. 935-939, https://doi.org/10.1038/nature04592.

[7] J. Wang, J. Y. Yang, I. M. Fazal, N. Ahmed, Y. Yan, H. Huang, Y. Ren, Y. Yue, S. Dolinar, M. Tur, A. E. Willner, Terabit Free-Space Data Transmission Employing Orbital Angular Momentum Multiplexing, Nature Photonics, No. 6, 2012, pp. 488-496, https://doi.org/10.1038/nphoton.2012.138.

[8] L. Zhu, A. Wang, J. Wang, Free-Space Data-Carrying Bendable Light Communications, Scientific Report, No. 9, 2019, pp. 14969, https://doi.org/10.1038/s41598-019-51496-z.

[9] S. Syubaev, A. Zhizhchenko, A. Kuchmizhak, A. Porfirev, E. Pustovalov, O. Vitrik, Yu. Kulchin, S. Khonina, S. Kudryashov, Direct Laser Printing of Chiral Plasmonic Nanojets by Vortex Beams, Journal of Physics: Conference Series, Vol. 951, 2018, pp. 012025, https://doi.org/10.1088/1742-6596/951/1/012025.

[10] Y. Zhang, M. Agnew, T. Roger, F.S. Roux, T. Konrad, D. Faccio, J. Leach, A. Forbes, Simultaneous Entanglement Swapping of Multiple Orbital Angular Momentum States of Light, Nature Communications, No. 8, 2017, pp. 632, https://doi.org/10.1038/s41467-017-00706-1.

[11] H. Y. Tsai, H. I. Smith, R. Menon, Fabrication of Spiral-Phase Diffractive Elements Using Scanning-Electron-Beam Lithography, Journal of Vacuum Science & Technology B: Microelectronics and Nanometer Structures, No. 25, 2007, pp. 2068-2071, https://doi.org/10.1116/1.2806961.
[12] T. Jankowski, N. Bennis, P. Morawiak, D. C. Zografopoulos, A. Pakuła, M. Filipiak, M. Słowikowski, J. M. López. Higuera, J. F. Algorri, Optical Vortices by An Adaptive Spiral Phase Plate, Optics & Laser Technology, Vol. 176, 2024, pp. 111029, https://doi.org/10.1016/J.OPTLASTEC.2024.111029.
[13] Y. H. Kim, C. Y. Hwang, J. H. Choi, J. E. Pi, J. H. Yang, S. M. Cho, S. H. Cheon, G. H. Kim, K. Choi, H. O. Kim, W. J. Lee, H. B. Kang, C. S. Hwang, Development of High-Resolution Active Matrix Spatial Light Modulator, Optical Engineering, Vol. 57, No. 6, 2018, pp. 1, https://doi.org/10.1117/1.oe.57.6.061606.
[14] A. S. Ostrovsky, C. R. Parrao, V. Arrizón, Generation of the Perfect Optical Vortex Using A Liquid-Crystal Spatial Light Modulator, Optics Letters, Vol. 38, Issue 4, 2013, pp. 534-536, https://doi.org/10.1364/ol.38.000534.
[15] K. Qu, Q. Jia, N. J. Fisch, Plasma Q-Plate for Generation and Manipulation of Intense Optical Vortices, Physical Review E, Vol. 96, No. 5, 2017, pp. 053207, https://doi.org/10.1103/PhysRevE.96.053207.
[16] D. W. Prather, J. N. Mait, M. S. Mirotznik, Design of Binary Subwavelength Diffractive Lenses by Use of Zeroth-Order Effective-Medium Theory, Journal of the Optical Society of America A, Vol. 16, Issue 5, 1999, pp. 1157-1167, https://doi.org/10.1364/JOSAA.16.001157.
[17] A. Filipkowski, Fabrication and Integration of Nanostructured Optical Devices, Engineering and Physical Sciences, 2015, http://hdl.handle.net/10399/4073 (accessed on: July 30th, 2025).
[18] K. Switkowski, A. Anuszkiewicz, A. Filipkowski, D. Pysz, R. Stepien, W. Krolikowski, R. Buczynski, Formation of Optical Vortices with All-Glass Nanostructured Gradient Index Masks, Optics Express, Vol. 25, No. 25, 2017, pp. 31443, https://doi.org/10.1364/oe.25.031443.
[19] F. Hudelist, J. M. Nowosielski, R. Buczynski, A. J. Waddie, M. R. Taghizadeh, Nanostructured Elliptical Gradient-Index Microlenses, Optics Letters, Vol. 35, Issue 2, 2010, pp. 130-132, https://doi.org/10.1364/ol.35.000130.
[20] R. Kasztelanic, N. T. Hue, D. Pysz, H. Thienpont, T. Omatsu, R. Buczynski, Free-form Optical Fiber with A Square Mode and Top-Hat Intensity Distribution, Advanced Science, Vol. 11, Issue 33, 2024, pp. 2402886, https://doi.org/10.1002/advs.202402886.
[21] N. T. Hue, K. Switkowski, R. Kasztelanic, A. Anuszkiewicz, Optical Characterization of Single Nanostructured Gradient Index Vortex Phase Masks Fabricated by the Modified Stack-And-Draw Technique, Optics Communications, Vol. 463, 2020, pp. 125435, https://doi.org/10.1016/j.optcom.2020.125435.
[22] N. T. Hue, L. V. Bau, C. V. Bien, T. T. Hai. L.V. Hieu, R. Kasztelanic, R. Buczynski, Achromatic Nanostructured Phase Components for Micro-Optical Vortex Beam Generation, Journal of the Optical Society of America B, Vol. 42, Issue 6, 2025, pp. 1194-1203, https://doi.org/10.1364/JOSAB.555732.
[23] CDGM, (n.d.). https://www.cdgmgd.com//database/toWebDatabase.htm?k=Products_Data&url=database (accessed on: July 30th, 2025).
[24] F. Hudelist, R. Buczynski, A. J. Waddie, M.R. Taghizadeh, Design and Fabrication of Nano-Structured Gradient Index Microlenses, Optics Express, Vol. 17, No. 5, 2009, pp. 3255-3263, https://doi.org/10.1364/oe.17.003255.
[25] R. Buczynski, A. Filipkowski, B. Piechal, N. T. Hue, D. Pysz, R. Stepien, A. Waddie, M.R. Taghizadeh, M. Klimczak, R. Kasztelanic, Achromatic Nanostructured Gradient Index Microlenses, Optics Express, Vol. 27, No. 7, 2019, pp. 9588, https://doi.org/10.1364/oe.27.009588.
[26] N. T. Hue, R. Kasztelanic, A. Filipkowski, D. Pysz, L.V. Hieu, R. Stepien, T. Omatsu, W. Krolikowski, R. Buczynski, Broadband Optical Vortex Beam Generation Using Flat-Surface Nanostructured Gradient Index Vortex Phase Masks, Scientific Reports, No. 13, 2023, pp. 20255, https://doi.org/10.1038/s41598-023-46871-w.
[27] K. Okamoto, Fundamentals of Optical Waveguides, Academic Press, 2006, pp. 329-383.